Single Molecule Studies of Dynamics in Polymer Thin Films and at Surfaces: Effect of Ambient Relative Humidity

Yanwen Hou and Daniel A. Higgins*

Department of Chemistry, Kansas State University, Manhattan, Kansas 66506

Received: May 14, 2002; In Final Form: July 25, 2002

The temporal emission characteristics of nile red (NR) single molecules in and on hydrophilic and hydrophobic polymer films are studied as a function of ambient relative humidity (RH), and hence, the film hydration level. The materials studied include poly(vinyl alcohol) (PVA) and poly(methyl methacrylate) (PMMA). The temporal emission characteristics for NR in and on PVA are shown to be very sensitive to the ambient RH. Autocorrelation of the single-molecule fluorescence transients reveal signal fluctuations on two distinct time scales: 0.1−1 s and 1−2 ms. The fast fluctuations become slower and the slow fluctuations faster with increasing RH. In stark contrast, data obtained from NR in and on PMMA show these films to be almost completely insensitive to ambient moisture. These results point to the important role played by material hydrophilicity in the sensitivity of single-molecule experiments to RH variations. The chemical and physical origins of the RH-dependent signal fluctuations are explored in detail. Triplet blinking is shown to be the dominant contributor to the fast signal fluctuations for dry films only. Rotational and translational molecular motions are observed to occur more frequently at higher RH. However, it is shown they are not the dominant causes of most signal fluctuations. It is concluded most of the signal fluctuations involve RH-dependent variations in the local molecular environment, which lead to time-dependent variations in the NR emission yield. These variations result from participation of a nonfluorescent twisted intramolecular charge-transfer state in the most polar, hydrated film regions.

I. Introduction

Recent advances in optical microscopy have enabled the location and spectroscopic interrogation of single molecules. New applications of single-molecule spectroscopy (SMS) are demonstrated regularly.[1−4] One common application is in the characterization of nanoscopic environments.[1,5−10] In our laboratory, we have sought to improve on current SMS methods so that semiquantitative spectroscopic information on nanoscale thin film properties can be obtained.[8−10] In previous work, we have employed an extension of Marcus theory for charge-transfer spectra[11,12] to obtain information on the nature of the nanoenvironments found in poly(vinyl alcohol) (PVA) and poly(methyl methacrylate) (PMMA) thin films[10] and in organically modified silicate glass films.[8,9] The strongly solvent-sensitive dye nile red[13] (NR) was used in these studies. Information on the local environment (solvent) reorganization energy was obtained, along with a measure of the solvent-relaxed transition energy.

In all of these previous studies, it was found that residual solvent (i.e., water) present in the films significantly altered the behavior of the single molecules. As in most single-molecule experiments, the initial step in sample characterization involved the recording of fluorescence images to locate the single molecules. In the presence of residual water, these images showed many fluorescent streaks, rather than the characteristic round fluorescent spots of diffraction-limited size usually observed in images of "dry" samples. Likewise, for the hydrophilic materials (i.e., PVA and some silicates), a transition from round spots to streaks was observed as the ambient laboratory humidity increased.[10] Such behavior is indicative of increased temporal variability in the nanoscale environments in which the single molecules reside. The moisture in the air determines the evaporation rate of the water used in preparation of PVA and silicate films. The equilibrium water content is also determined by the ambient humidity and material hydrophilicity. As a result of these initial observations, all subsequent experiments have been performed under conditions designed to maintain approximately constant ambient humidity and, hence, constant film moisture.

It is indeed well-known that atmospheric moisture is readily adsorbed on hydrophilic surfaces and in hydrophilic surface coatings.[14−24] The latter effect is manifested most dramatically in the swelling of polymer films in humid environments.[22,23] The presence of water vapor in the environment can dramatically alter the friction, adhesion, and lubrication properties of these films and their surfaces.[18,24,25] In the laboratory, thin liquid films on surfaces, and the associated capillary forces, are known to be important in surface forces measurements[26] and in chemical force microscopy experiments.[27,28] Ultrathin films of water formed on surfaces under high humidity have also recently been utilized to allow imaging of biomolecules by scanning tunneling microscopy on otherwise insulating substrates.[19−21]

Although the importance of atmospheric moisture in SMS studies was realized previously,[10] its effects on local film properties, and hence single-molecule observables, have not been previously studied in detail. In this publication, it will be shown that adsorption of atmospheric moisture on hydrophilic surfaces and in hydrophilic thin films can dramatically alter the results of single-molecule experiments. The present work differs from our previous studies in that it deals entirely with moisture-

* Corresponding author. E-mail: higgins@ksu.edu.

10.1021/jp021200v CCC: $22.00
Published on Web 09/11/2002

dependent fluorescence signal fluctuations in the time domain, and their possible origins. These signal fluctuations are the cause of the image streaks described above. Dynamical processes shown to vary with ambient humidity include translational and rotational molecular motions. The moisture dependence of triplet blinking phenomena,[29−32] spectral diffusion,[33,34] and time-dependent variations in the emission quantum yield are also explored. Emission yield variations are attributed here to the freeing of low-frequency intramolecular motions in NR by nanoscopic changes in the thin film environment. Hydration of the single-molecule environments allows more frequent excitation of NR to a nonfluorescent twisted intramolecular charge-transfer (TICT) state.[35−37]

II. Experimental Considerations

A. Sample Preparation. Nile red (NR), poly(methyl methacrylate) (PMMA), poly(vinyl alcohol) (PVA), and all organic solvents (spectrophotometric grade) were obtained from Aldrich. Except for PVA, all materials were used as received. PVA was purified by reprecipitation from aqueous solution (using acetone) and was thoroughly dried by gently heating under vacuum until the system pressure reached 30−60 mTorr.

Polymer films were prepared in two different ways to produce samples in which the dye was present (i) primarily on the film surface and (ii) entrapped within the polymer films. In the first method, polymer solution was first spin cast onto clean glass microscope cover slips (Fisher Premium). Films a few hundred nanometers in thickness were obtained. One drop of 10^{-9} M methanolic NR solution was then spin cast on top of the preformed polymer film. In the second method, the films were prepared by spin casting a homogeneous solution of NR and polymer on the glass substrate. PMMA films were prepared from 4 mg/mL methylene chloride solution, whereas PVA was cast from a 50 mg/mL aqueous solution. High-purity water (18 MΩcm water) was used for preparation of the PVA solution.

To investigate the effects of atmospheric moisture on the samples, a sealed box was used to cover all samples prior to and during single-molecule experiments. The relative humidity (RH) inside the box was increased to controlled levels above ambient (≈30% RH, 22 °C) by evaporation of high-purity water at room temperature inside the box. The humidity within the box was continuously monitored to ±1% with a small hygrometer (Control). A dry atmosphere was obtained by purging the box with nitrogen gas. Samples were allowed to equilibrate for at least one-half hour prior to each experiment and following a change in humidity.

B. Instrumentation. Single-molecule images and spectrally integrated time-dependent fluorescence signal traces (fluorescence transients)[29,30,38] were acquired using a home-built sample scanning confocal microscope. This microscope has been described previously.[8] Briefly, samples were mounted on a scanning stage (Queenstage) that utilizes closed-loop X,Y feedback. The sample stage was mounted on an inverted, epi-illumination microscope (Nikon, TE-200). Light from either a green HeNe laser (543.5 nm) or an argon ion laser (514.5 nm) was used to excite the NR molecules. The power into the microscope was maintained between 0.2 and 1.5 μW in most experiments.

Prior to directing it into the microscope, the laser beam size and divergence were adjusted by use of a telescope. Narrow band-pass filters were employed in the excitation path to ensure no radiation from other plasma lines entered the microscope. A polarization scrambler was used to produce unpolarized light for orientation insensitive (in the sample plane) excitation of the single molecules. Finally, the excitation light was reflected from a dichroic beam splitter (Chroma) into the back aperture of a 100×, 1.3 numerical aperture oil immersion objective (Nikon). The incident laser beam size just filled the back aperture of the objective. The dichroic beam splitter repolarized the incident light to a small degree. The objective produced a nearly diffraction-limited, 300 nm diameter focus on the sample.

The same objective was used to collect fluorescence from the single molecules. The collected fluorescence passed back through the dichroic beam splitter. Appropriate notch (Kaiser Optical) and band-pass (Chroma) filters were used to isolate the single-molecule fluorescence from residual excitation light. Single-molecule fluorescence was detected using single-photon-counting avalanche diodes (Perkin-Elmer).

Fluorescence transients were recorded using either one single-photon-counting avalanche diode (for monitoring the total single-molecule emission) or a polarizing beam-splitter cube (CVI) and two avalanche diodes (for monitoring the two orthogonal, in-plane components of polarized single-molecule emission). In many cases, data from the two signal channels (representing the two polarization components) were summed to obtain data equivalent to the unpolarized emission transients recorded with a single detector. Dwell times of 0.5−10 ms were employed in these experiments, as defined below in the discussion of individual studies.

Spectral diffusion phenomena[33,34] were investigated by directing the single-molecule emission into a 0.15 m imaging spectrograph and associated liquid-N_2-cooled CCD detector (Roper Scientific). Using this system, numerous emission spectra were recorded for each single molecule by integrating the fluorescence for 0.25 s. Sequential spectra were separated by 1.2 s by the time required to read the detector array.

Time-dependent studies of single-molecule translational diffusion were performed by wide-field illumination methods.[39,40] For these studies, a lens was inserted in the excitation beam path so that the beam was focused near the back aperture of the objective. The microscope objective then produced an illuminated sample area of approximately 700 μm^2. To record fluorescence images, the CCD described above was moved into the primary image plane of the microscope and illuminated with the fluorescence collected from the sample. The pixel size in the CCD chip is 20 μm × 20 μm, giving a pixel resolution at the sample of approximately 200 nm. For collection of these images, the fluorescence signal was integrated for 1.0 s. Multiple images of the same sample area were recorded sequentially at 1.4 s intervals, as defined by the time required to read the CCD detector array.

III. Results and Discussion

A. Imaging and Fluorescence Transients. Figure 1 depicts representative fluorescence images recorded under different ambient conditions for PMMA and PVA films with NR coated on top. The chemical structure of NR is also given. At low RH (≈30%), bright round fluorescent spots of diffraction-limited size were observed for both materials. These spots were attributed to emission from single NR molecules, on the basis of a number of well-known criteria.[3,4] As the RH was increased, the two samples exhibited distinctly different behavior. For PMMA, even in very humid environments (RH ≈ 90%), the images showed only subtle changes (compare Figure 1A,B) in NR emission behavior. In contrast, the images for NR on PVA changed from bright round spots to predominantly streaks (compare Figure 1C,D) starting at ≈75% RH. The appearance of the image streaks is a manifestation of the dramatic increase

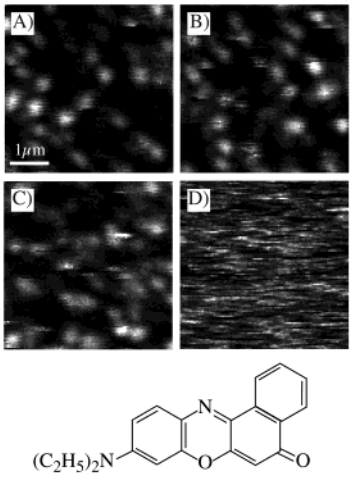

Figure 1. Representative images recorded for (A) NR on a PMMA film at 30% RH, (B) approximately the same area at 90% RH, (C) NR on a PVA film at 30% RH, and (D) approximately the same area at 78% RH. The chemical structure of NR is also shown. Some positional drift occurred between the recording of images A and B. The relative intensities of some of the spots also changed between the two images.

in the frequency and amplitude of time-dependent signal fluctuations that occur for the single molecules.

The lack of variation in the images of NR-doped PMMA with increasing ambient RH can be explained by the relatively hydrophobic nature of PMMA. The solid PMMA films provide a dry (i.e., no water), nominally static[10] environment for the single molecules under all conditions explored. Atmospheric moisture does not interact with the PMMA, and hence, single-molecule experiments on PMMA are insensitive to variations in ambient humidity. PVA also provides a static environment for the single molecules under low humidity conditions, for which the films are relatively dry. In our previous study,[10] it was shown that the highly cross-linked, hydrogen-bonded structure of dry PVA films incorporate substantially more rigid environments than do PMMA films. The hydrogen-bonded structure of the film is, however, readily broken up by incorporation of water.[22] PVA swells appreciably in a wet environment as water molecules insert in the hydrogen bonds between the polymer chains. Under the humid conditions of Figure 1D (78% RH), significant amounts of water are adsorbed on and in the film, yielding substantially more fluid nanoenvironments that allow for greater molecular mobility. The streaks are observed in the images for a number of specific reasons, as is explored in detail below. Similar effects are expected and observed[41] for hydrophilic glass substrates routinely used in singe-molecule experiments.[6]

The data shown in Figure 1 depict the RH-dependent variations observed when single molecules are deposited on sample surfaces. It is also interesting to observe the effects of ambient humidity variations as a function of the location of the dye with respect to the film surface (i.e., in vs on the films). Figure 2 presents results comparing films prepared with NR molecules entrapped in PVA films (left column of images) and deposited on the films (right column). As is readily apparent, there are substantially more signal fluctuations observed for the molecules on the film at each RH level. This is most likely due to the greater accessibility of the surface environments and surface-adsorbed molecules to moisture.

To better quantify the time scales for the single-molecule signal fluctuations, fluorescence time transients were recorded for individual fluorescence spots as a function of RH. At high

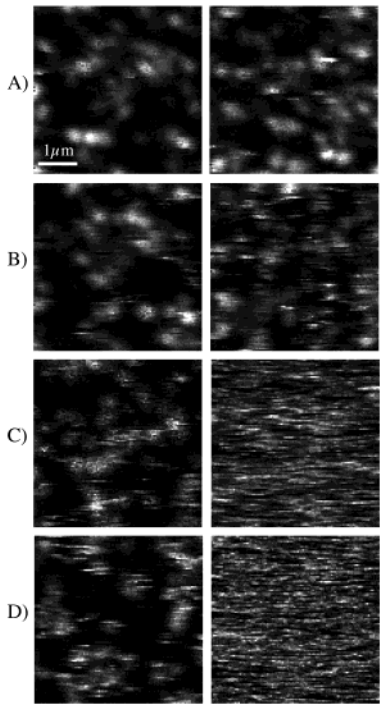

Figure 2. Representative images for NR in PVA films (left column) and on PVA films (right column). The images were recorded at (A) 25% ± 1%, (B) 58% ±1 %, (C) 76% ± 2%, and (D) 92% ± 3% ambient RH.

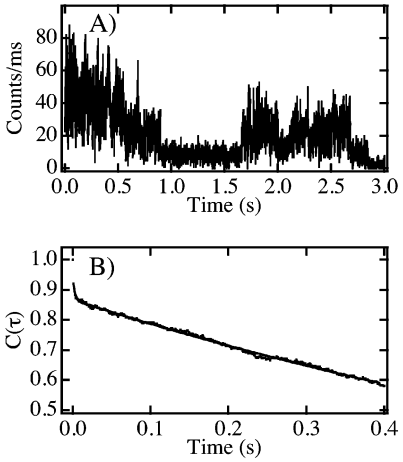

Figure 3. (A) Spectrally integrated time-dependent fluorescence transient of a NR molecule entrapped in PVA at 65% RH. (B) Autocorrelation function of the data in (A) and the double exponential fit. The data were recorded with 1 ms time resolution.

RH the transients were recorded by focusing on individual sample regions where streaks were observed. Figure 3 shows an example of such a transient. Quantitative information was obtained from these data by performing an autocorrelation analysis. Autocorrelation analysis has been described previously, in detail.[6,30,38] The autocorrelation function employed is given as

$$C(\tau) = \frac{\frac{1}{N-\tau}\sum_{t=1}^{N} S(t)\, S(t+\tau)}{\frac{1}{N}\sum_{t=1}^{N} S(t)^2} \qquad (1)$$

The value of the autocorrelation function, *C*, is calculated for

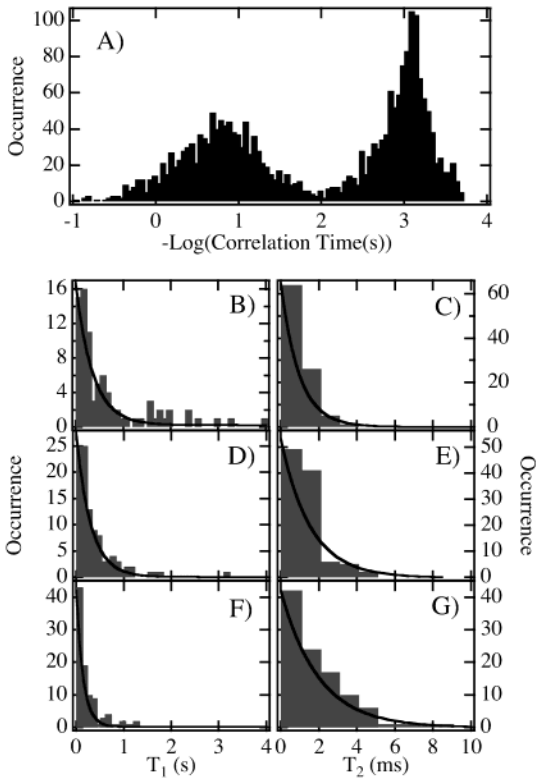

Figure 4. Histograms of the correlation times obtained by fitting the autocorrelation functions calculated from fluorescence time transients of NR in PVA films. (A) Compilation of all correlation times. (B), (C) Slow and fast correlation time histograms at 31% RH. (D), (E) Slow and fast correlation time histograms at 65% RH. (F), (G) Slow and fast correlation time histograms at 86% RH.

discrete time displacements τ of the fluorescence transients $S(t)$ of length N. The results for the data in Figure 3A are shown in Figure 3B.

It was found that the autocorrelation functions for all recorded time transients could be fit reasonably well to double exponential decays. In some cases, the data fit well to a single exponential. The specific function used to fit the data is given as

$$C(\tau) = A + B_1 \exp\left[-\frac{\tau}{T_1}\right] + B_2 \exp\left[-\frac{\tau}{T_2}\right] \qquad (2)$$

Here, T_1 and T_2 represent the characteristic time scales for the decay of $C(\tau)$. The spike at zero time in each $C(\tau)$ (see Figure 3) is due to uncorrelated measurement noise (i.e., shot noise) and other signal fluctuations that are much faster than the time resolution of the data. It was therefore excluded from the fitting procedure. Only the initial 10%, out to a maximum of about 2 s, of each $C(\tau)$ decay was fit. It is well-known that there are insufficient data at longer time scales to provide statistically meaningful results in short transients.[6]

Figure 4 shows the final statistical results of the autocorrelation analysis. Shown in Figure 4A is a histogram incorporating all T_1 and T_2 values obtained from autocorrelations performed on more than 1000 single-molecule transients. It is clear from these data that there are two distinct time scales for the signal fluctuations. Included are fast signal fluctuations that yield a signal correlation decay time near 1 ms and much slower fluctuations in the 0.1−1 s range. The shorter of the two decay times obtained from the biexponential fits was sometimes less than the time resolution of the experiment. These data were excluded from the full analysis and interpretation presented below.

TABLE 1: Autocorrelation Analysis Results for the Fluorescence Transients at Different RH Levels[a]

	31% ± 1%	65% ± 2%	86% ± 3%
T_1 (s)	0.4 ± 0.3	0.31 ± 0.09	0.15 ± 0.06
$T_{A,1}$ (s)	0.3 ± 0.3	0.25 ± 0.09	0.12 ± 0.06
$T_{B,1}$ (s)	0.3 ± 0.3	0.3 ± 0.2	0.18 ± 0.06
T_2 (ms)	1.0 ± 0.1	1.6 ± 0.2	2.0 ± 0.3
$T_{A,2}$ (ms)	1.0 ± 0.1	1.6 ± 0.2	2.0 ± 0.3
$T_{B,2}$ (ms)	1.1 ± 0.2	1.4 ± 0.1	2.0 ± 0.3

[a] T_1 and T_2 represent the average signal correlation decay times obtained from unpolarized total-fluorescence transients. $T_{A,1}$, $T_{B,1}$, $T_{A,2}$, and $T_{B,2}$ represent the average slow (1) and fast (2) signal correlation decay times obtained from orthogonally polarized emission signals (arbitrarily labeled A and B). The error bars represent the 95% confidence intervals on each value.

For subsequent data analysis, the individual autocorrelation decay times were divided into "fast" and "slow" components. On the basis of the data shown in Figure 4A, a threshold of 10 ms was used in making the determination of whether a particular T represented slow (T_1) or fast (T_2) signal fluctuations. Individual histograms were then constructed from the measured autocorrelation decay times at each ambient RH level. Parts B−G of Figure 4 give these data.

Each histogram in Figure 4B−G can be fit with a single exponential to obtain the average signal correlation times for each sample. These correlation times are tabulated in Table 1. From Figure 4 and Table 1, it is clear that the rate of the slow signal fluctuations increases substantially (by a factor of about 2.5) as the humidity is increased. At low RH (31%), the slow fluctuations occur with an average T_1 of 0.4 s. At high RH (86%) an average fluctuation time of 0.15 s is measured. In contrast, the apparent rate of the fast signal fluctuations actually decreases by a factor of about 2 as the humidity is increased. At low RH, the average autocorrelation function decays with $T_2 = 1$ ms and at high RH the decay occurs on a 2 ms time scale. This strong humidity dependence reveals that adsorbed atmospheric moisture has a profound influence on dynamical single-molecule processes occurring in hydrophilic thin films.

B. Molecular Origins of Signal Fluctuations. Numerous studies have reported measurements of the thickness of water layers adsorbed on hydrophilic surfaces from humid air.[14−16] For perfectly hydrophilic surfaces (as determined by contact angle measurements), the thickness of the water layer can be more than 100 nm.[16] Therefore, a relatively thick layer of water is expected on PVA at the highest humidities. However, as PVA and water are mutually soluble, a substantial amount of water is also expected to penetrate the surface and migrate into the film. Insertion of water molecules in the hydrogen-bonded polymer matrix causes the film to swell.[22,23] Although time is required for the uptake of moisture by these films, their ultimate hydration levels at equilibrium are determined by the relative level of moisture in the air.[14−16]

Detailed knowledge on the molecular-scale origins of the humidity-dependent signal fluctuations will yield a better understanding of the molecular-level changes that occur in thin films and on surfaces with increased material hydration. Such studies may also help us to better understand the photophysical phenomena associated with commonly observed single-molecule emission fluctuations.[6,7,9,29,30,32,38,42] There are several possible reasons for the increased single-molecule emission fluctuations observed with increasing ambient RH. These are discussed below.

The most obvious possible origins for the signal fluctuations are those dealing with triplet blinking,[29] and simple physical

motions of the molecules (i.e., rotational and translational diffusion). Greater molecular mobility results from enhanced fluidity of the environments themselves with hydration of the film. Intramolecular motions (i.e., rotation of the NR diethylamine group) may also be enhanced in more fluid environments. Because these motions are associated with the formation of a nonfluorescent TICT excited state,[35−37] they likely lead to dramatic humidity-dependent variations in the quantum yield for emission. These more subtle effects, and their manifestations at the single-molecule level are of most interest here.

1. Triplet Blinking. It is well-known that upon electronic excitation, a dye molecule can undergo intersystem crossing to a relatively long-lived triplet excited state. Once in the triplet state, the molecule cannot be further excited (at the same wavelength)[43] and does not fluoresce. Once the molecule relaxes to the ground state, it can again be excited and fluorescence is observed. Such "triplet blinking" has been described on a number of occasions.[29−32,43] It is clear that triplet blinking contributes to some of the signal fluctuations reported here. To investigate the extent of its contributions, emission transients (unpolarized) were recorded for individual molecules excited at different intensities. Results were only obtained under low RH conditions. At higher RH, other mechanisms appeared to dominate the fluctuations (see below).

The emission transients obtained were analyzed by first preparing histograms of the emission signal. A representative example is shown in Figure 5. It is clear from these histograms that there are at least two different signal levels. Either the molecule is nonemissive and only background counts are detected, or it is emitting and some relatively large fluorescence signal is detected. Often, different levels of fluorescence are observed, beyond those expected for simple shot-noise limited fluctuations. The histogram shown in Figure 5B depicts the dark and emissive states via the appearance of two peaks in the histogram. From such histograms, a threshold value is selected (i.e., the local minimum between the dark and emissive states) for classifying the molecule as either being emissive or nonemissive. This threshold value is then used to calculate "on times" and "off times" from the fluorescence transient.[30,43] Each "on time" corresponds to the length of time the molecule spends cycling between the ground and excited states in the singlet manifold. Each "off time" corresponds to the time the molecule spends in the dark triplet state.

Parts C and D of Figure 5 show frequency distributions of these "on times" and "off times" for a single NR molecule in PVA at low RH, as a function of excitation intensity. The average "on time" and average "off time" for a given molecule are obtained by fitting these data to single-exponential decays; these fits are also plotted in Figure 5. As is readily apparent, the "on times" for this molecule get monotonically shorter as the excitation intensity is increased, yielding values of 4.0, 2.9, and 2.0 ms for incident powers of approximately 1, 3.2, and 6.5 μW, respectively. This behavior is clear evidence that the transition to the dark state is photoinduced and likely involves intersystem crossing to the triplet state. In contrast to the "on times", the "off times" are independent of excitation intensity and are all in the 0.4 ± 0.1 ms range. The 1 ms signal correlation decay time reported above for NR in PVA films at low RH is therefore consistent with, and attributable to, the effects of triplet blinking. Autocorrelation of these same fluorescence transients showed the same power-dependent trend for the fast (T_2) fluctuations but no clear trend for the slow (T_1) fluctuations.

At higher RH, the apparent rate of the fast fluctuations decreases (see Table 1). The decrease in fluctuation rate may

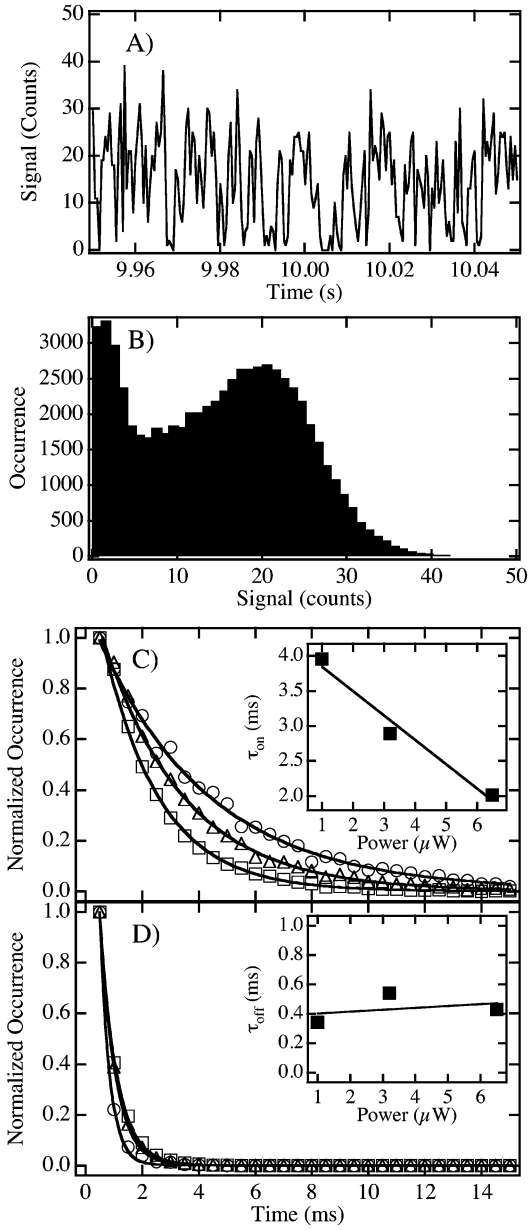

Figure 5. (A) Representative fluorescence transient (0.5 ms resolution, expanded region) for a single NR molecule in PVA at low RH. (B) Histogram of signal levels for the entire fluorescence transient in (A). (C) Frequency distribution in τ_{on} for one molecule at incident powers of approximately 1 (circles), 3.2 (triangles), and 6.5 μW (squares). The inset shows the average τ_{on} determined by fitting these data to single-exponential decays. (D) Frequency distribution in τ_{off} for the same single molecule. The inset shows the average τ_{off} values for each.

have several origins. If sufficient time resolution is available to faithfully record the triplet lifetime, the lengthening of the signal correlation time could reflect an increase in the "on time" (i.e., a decrease in the intersystem crossing rate) and/or an increase in the triplet lifetime. However, as the triplet lifetime reported above (0.4 ms) is already at the limit of our time resolution, it is believed the observed increase in signal correlation time actually reflects a decrease in the triplet lifetime. Indeed, such a decrease in lifetime is expected and is attributable to an increase in the mobility of NR and dissolved oxygen in the more hydrated films. It is well-known that the triplet lifetimes of most dyes (including NR) are shorter in the presence of mobile O_2.[42,44,45] The ground state of O_2 is a triplet and readily quenches the triplet excited state of the dye.

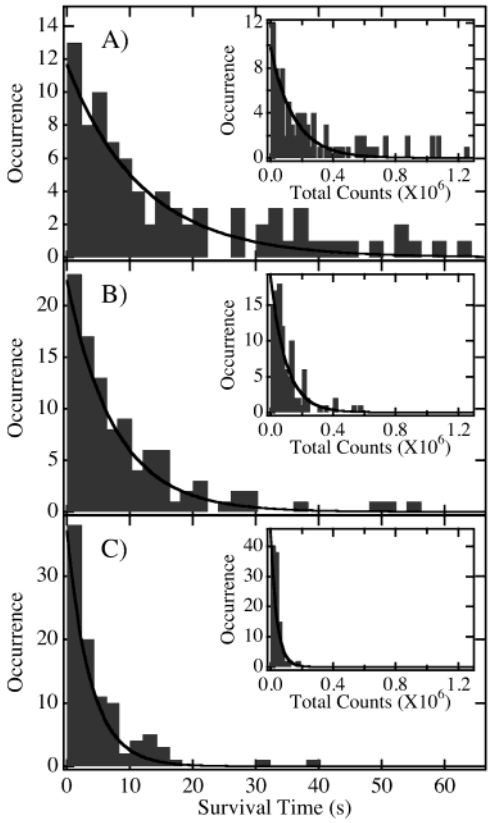

Figure 6. Histograms of survival times for Nile Red in PVA at (A) 31%, (B) 65%, and (C) 86% RH, respectively. The insets show the corresponding histograms of total photons emitted.

Singlet O_2 is produced during the quenching of the NR triplet. Further reaction of the dye with singlet O_2 leads to irreversible photochemical destruction of the dye. Therefore, additional evidence for the role played by the triplet can be obtained from observations of the humidity-dependent survival time of the single molecules. Figure 6 presents histograms of the total survival times[46] measured for NR molecules in PVA. These times were determined by simply measuring the length of time elapsed between the start of a fluorescence transient and the point at which the molecule's fluorescence dropped permanently to the background level in a discrete event. Molecules showing clear evidence of diffusion (see below) were explicitly excluded from this analysis. Single-exponential fits of these histograms show a decrease in average survival time with increased RH, giving values of 12 ± 1, 7.6 ± 0.5, and 3.7 ± 0.2 s for 31%, 65%, and 86% RH environments, respectively. Also shown in Figure 6 are histograms of the total number of photons detected from each molecule prior to photobleaching. The average number of photons detected under these same conditions was 1.2×10^5, 1.0×10^5, and 4.0×10^4, respectively.

These results clearly prove the molecules are more readily photobleached in the more hydrated films. They also support the conclusion that the triplet lifetime is shortened (because of enhanced O_2 quenching) under higher RH conditions. Therefore, it may be concluded that triplet blinking does not play a significant role in the RH dependence of the single-molecule signal fluctuations in any of the hydrated films.

2. Translational Diffusion. Translational motions of the single molecules in and on the hydrated films are expected[47] and will contribute to the fluctuations in the fluorescence transients. Such fluctuations result simply from the migration of molecules in and out of the illumination volume of the microscope. As film moisture increases with increasing RH, such motions occur more frequently, yielding more signal fluctuations. The data presented in Figure 7 indicate that molecular translational motion is indeed observable. These images were recorded for a single sample area under dry ambient conditions (RH$\approx$ 30%). However, in the time between the recording of these two images, the RH was increased to about 86%. The sample was held under these conditions for about 1 h, at which point an image was recorded (not shown). Its appearance is very similar to that shown in Figure 1D. As shown by the data (compare Figure 7A,B), a few single molecules (labeled by arrows) appear at almost the same positions in both images, whereas many other molecules appear to have moved to new positions. It is also possible that the bright spots observed in similar places in both images are not the same molecules. Rather, they may be other molecules that for some reason preferentially adsorb (or are otherwise trapped) in these specific locations.[47]

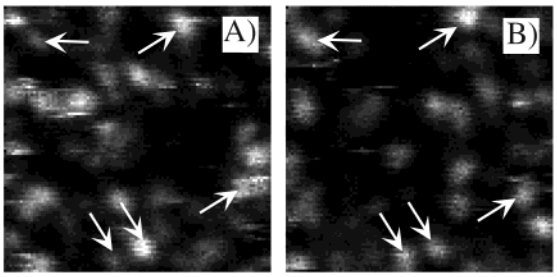

Figure 7. (A) Image of NR on PVA at 30% RH. (B) Image of the same area recorded after the ambient RH had been increased to 86% for approximately 1 h and subsequently reduced to 30%. Examples of molecules that appeared to remain in the same positions throughout the experiment are highlighted on the images.

It is difficult to obtain quantitative information on the diffusion coefficient for the molecules using sample scanning confocal methods (as in Figures 1, 2, and 7) as the molecules *appear* to move too rapidly at high RH. However, an upper limit for the average single-molecule diffusion coefficients can be estimated from the fluorescence transients. The autocorrelation analysis discussed above may be used for this purpose, assuming the decay of $C(\tau)$ is dominated by the effects of translational diffusion. In this instance, the values reported in Table 1 for T_1 (or T_2) would represent the average residence time of a single molecule in the detection volume. The molecular motion is then related to the diffusion coefficient by

$$\Delta r = \sqrt{2Dt} \tag{3}$$

Here, Δr represents the half-width of the Gaussian excitation profile (the beam focus) in the sample and t is the average residence time in the focus. From the T_1 data reported in Table 1, average diffusion coefficients of 3×10^{-10} and 4×10^{-10} cm^2/s are estimated for films studied at 31% and 65% RH, respectively. From T_2, average diffusion coefficients of 1×10^{-7} and 7×10^{-8} cm^2/s are estimated at these same RH levels. The diffusion coefficient obtained from T_1 increases to 8×10^{-10} cm^2/s at 86% RH, whereas that obtained from T_2 decreases to 6×10^{-8} cm^2/s.

The diffusion coefficients estimated from T_2 may be rejected for several reasons. Most notable are the counterintuitive trend in D with increasing film moisture, and the fact that permanent bleaching transitions are observed at the end of each transient on much longer time scales. The latter observation is most consistent with relatively slow diffusion. Those estimated from T_1 cannot be rejected as readily. However, the values are suspect,

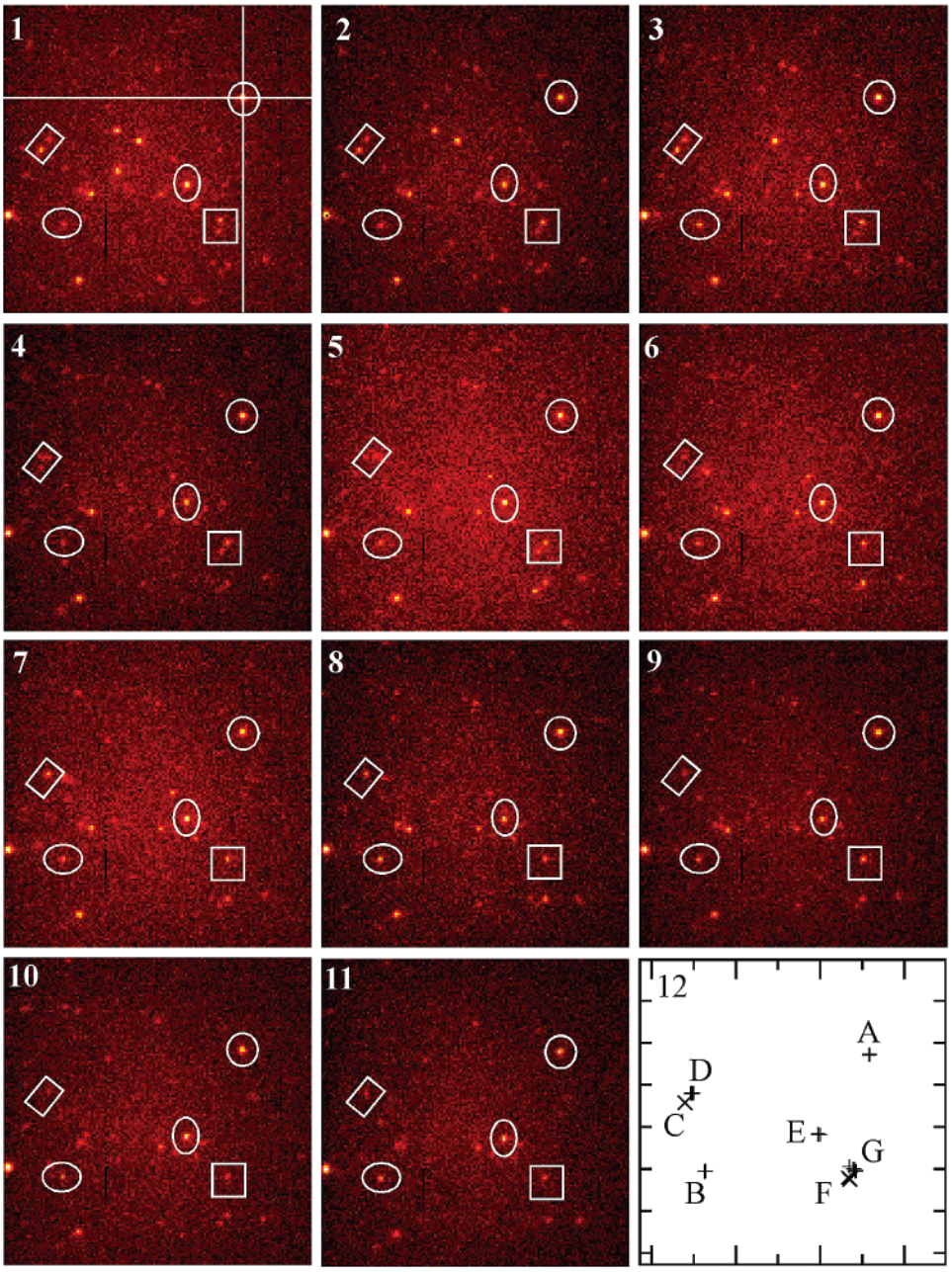

Figure 8. (1−11) Single-molecule broad illumination images of NR molecules in PVA at about 82% RH. The integration time for each image is 1 s. The time interval between consecutive images is 1.4 s. Frames and circles are used to highlight molecules of particular interest. Single-molecule positions are obtained by curve fitting the intensity profile for each molecule along two dimensions, as depicted in (1). (12) Trajectories of the highlighted molecules.

as they suggest the molecules move only twice as fast in the hydrated films (on average) as in the dry films. Clearly, were all the signal fluctuations due to translational diffusion, this result would be inconsistent with the images reported in Figures 1 and 2, for which dramatic changes in the rate of molecular motions appear to occur with increased film hydration. That is, image streaks would be prevalent in *both* the dry and hydrated films.

An additional measurement of the diffusion coefficient at high RH can be obtained from wide-field illumination experiments.[39,40] Figure 8 shows a series of images recorded for an approximately 26 × 26 μm sample area at RH ≈ 82%. This region exhibited a relatively lower concentration of spots, making it easier to identify individual molecules. The images were recorded as described in the Experimental Section. The signal integration time for each image was 1.0 s, with 1.4 s between consecutive images. The center position of each molecule in each image was determined by previously published fitting procedures.[39,40] For this analysis, the intensity profile for each fluorescent spot was fit to a Gaussian function in each of two dimensions in the sample plane (i.e., x and y). The peak position of the Gaussian gives the coordinates of the molecule to high precision.[39,40] By combining the coordinate data for each molecule in each image, the motions of the individual molecules can be tracked. The molecular motions are observed to be extremely small in most cases, as evidenced by the single-molecule trajectories plotted in Figure 8. The observed root-mean-square (RMS) displacements of the individual spots from their original positions are tabulated in Table 2 for the labeled molecules, along with their calculated diffusion coefficients. With one exception, all yield diffusion coefficients in the 10^{-12}

TABLE 2: Summary of the RMS Displacements (nm) and Diffusion Coefficients D ($\times 10^{-13}$ cm^2/s) of the Molecules Highlighted in the Images Shown in Figure 8

	A	*B*	*C*	*D*	*E*	*F*	*G*
RMS	33	40	19	67	52	105	1600
D	2.2	3.2	2.1	9.0	5.3	52	5100

to 10^{-13} cm^2/s range. Molecule "G" exhibits much faster diffusion, yielding a diffusion coefficient of about 5×10^{-10} cm^2/s.

Taken together, the two sets of results (fluorescence transients and broad illumination data) indicate that translational diffusion is likely the dominant cause of the (sub)second signal fluctuations for only a relatively small fraction of the molecules at all RH levels. It is particularly noteworthy that the majority of diffusion coefficients measured in the broad illumination experiments are approximately a factor of 10^3 smaller than those estimated from the T_1 values. Therefore, it may be concluded that translational diffusion is not the dominant cause of the fluctuations observed in the fluorescence transients, as reflected by the measured T_1 and T_2 values. Again, this conclusion is supported by the observation of photobleaching transitions, followed by extremely long periods (seconds) of background signal for many sample regions, even under high RH conditions.

3. Rotational Diffusion. Besides translational diffusion, single-molecule rotational motions may also be contributing to the signal fluctuations.[7,48,49] Because the molecules are not efficiently excited if their transition dipoles rotate out of the sample plane,[7,50] such motions would cause substantial fluctuations. Though it is possible to obtain direct information on out-of-plane orientational motions of the single molecules, such measurements either require special far-field optical configurations[49,50] or near-field optical methods.[51] Interpretation of the data typically involves careful fitting of single-molecule emission patterns.[49,51] Such methods are not employed here. Rather, it is simply assumed that in-plane and out-of-plane motions are equally probable (i.e., the molecules are assumed to be entrapped in isotropic environments). The contributions of out-of-plane motions to the fluctuations can then be estimated from studies of the in-plane motions alone.

To investigate the effect of ambient RH on in-plane molecular rotations, polarization-dependent fluorescence transients were recorded. As described in the Experimental Section, a polarizing beam splitter was employed in the collection path of the microscope to divide the fluorescence into two orthogonal polarization components, representing two orthogonal polarization directions in the sample plane. The two resulting fluorescence signals were recorded simultaneously and are arbitrarily designated as A (detector A) and B (detector B). Hundreds of such polarization-dependent fluorescence transients were recorded under different humidity conditions. Figure 9 shows three representative sets of data.

At relatively low RH (≈30%), most of the transients behave similarly to the one shown in Figure 9A. The two signal components most often fluctuate in a correlated manner, neglecting fluctuations due simply to shot noise. Such molecules show no apparent in-plane rotational motion. It is concluded such molecules are entrapped in the films at fixed orientations (i.e., out-of-plane motions are also absent). The relatively rapid signal fluctuations observed in Figure 9A, again, are attributable primarily to triplet blinking.

As the humidity was increased to moderate levels (RH ≈ 65%), the majority of molecules studied produced two anticorrelated signal traces, a clear sign of in-plane molecular rotations.[7] Figure 9B presents a typical example. While the total signal level remain approximately constant, around 0.84 s, a slow change in molecular orientation occurred, leading to a decrease in the B polarization component and an increase in the A component. Rotations at moderate RH were usually slow, occurring on seconds or hundreds of millisecond time scales. In addition to such slow motions, rotational jumps[48] were also observed.

At the maximum RH studied (about 86%), rotations occurred more frequently and on relatively shorter time scales, as shown in Figure 9C. In these data, anticorrelated signal fluctuations are observed at 0.26, 0.28−0.30, 0.30−0.31, and 0.33 s, respectively. Most of these signal fluctuations are well outside those expected for shot noise. These fluctuations are attributed to in-plane molecular orientational motions occurring on 10^{-3} to 10^{-2} s time scales.

Quantitative analysis of the motions reflected by such polarization-dependent time transients usually involves calculation of the reduced linear dichroism.[7] Here, however, the goal is to deduce the extent to which out-of-plane molecular motions contribute to the signal fluctuations. Therefore, alternative methods were employed. Specifically, the autocorrelation decay times for the individual polarization components (A and B) were compared to those obtained from the total (unpolarized) fluorescence data. Histograms of the correlation times for each polarization component were prepared (not shown) and fit to exponential decays as in Figure 4. The average correlation times obtained from these fits are presented in Table 1.

The autocorrelation decay from a single detector (i = A or B) (i.e., for a single polarization component) is represented by eqs 4 for the case of a single-exponential decay. Here, T_{ipr} and

$$C_i(\tau) \propto \exp\left[-\frac{\tau}{T_r}\right] \qquad \frac{1}{T_r} = \frac{1}{T_{ipr}} + \frac{1}{T_{opr}} \tag{4}$$

T_{opr} are rotational correlation times associated with in-plane and out-of-plane rotations, respectively, and T_r is the total rotational correlation time. Again, T_{ipr} and T_{opr} are assumed to be equal. The autocorrelation decay for unpolarized fluorescence (i.e., the sum of the two detector signals) is given by

$$C_i(\tau) \propto \exp\left[-\frac{\tau}{T_{opr}}\right] \tag{5}$$

Equation 5 depends only on the time scale for out-of-plane reorientation. As a result, the autocorrelation functions derived from the polarized emission data should decay twice as fast as those from the unpolarized fluorescence transients, if rotational motions are the dominant cause of the fluctuations. As is apparent from Table 1, such is not the case. Both the polarized and total fluorescence signals exhibit similar correlation times for all samples studied. It may therefore be concluded that, on average, the in-plane rotational motions that are clearly observable (see Figure 9) are not the dominant cause of signal fluctuations in the individual polarization signals. Assuming there is no preference for out-of-plane molecular motions, it may also be concluded that out-of-plane motions are not the dominant cause of the signal fluctuations in the unpolarized fluorescence transients, at any of the RH levels studied.

4. Quantum Yield Fluctuations. The possible role played by variations in the fluorescence quantum yield is difficult to directly assess. However, NR and structurally related dyes (i.e., the coumarins[52]) are known to possess twisted-intramolecular charge-transfer (TICT) excited states.[35−37] For these dyes, formation of the TICT state involves transfer of nearly one quantum of charge from the electron-donating diethylamine

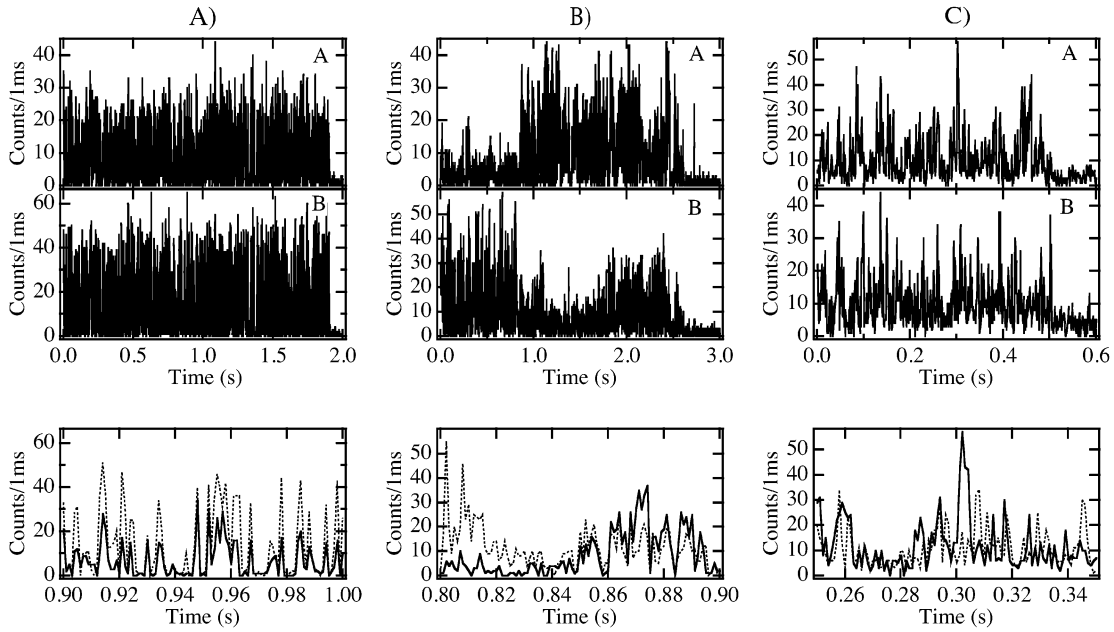

Figure 9. Representative fluorescence transients recorded for two orthogonal in-plane polarization components (top, arbitrarily labeled A and B) from NR single molecules in PVA films at (A) 31%, (B) 65%, and (C) 86% RH. Expanded sections of the data for the two polarization components [bottom: (solid) A, (dashed) B].

group onto the ring structure. Simultaneously, the diethylamine group rotates so that its nonbonding electronic orbital no longer couples with the conjugated π-electronic structure of the molecule. Radiative relaxation from the TICT excited state to the planar ground state is forbidden. As a result, a low fluorescence quantum yield is expected under circumstances in which the TICT state participates.[53]

The TICT state of NR is preferentially formed in more polar environments, as reflected by the dramatic decrease in its emission yield in polar solvents.[35−37] Any emission from the more polar TICT state would be red-shifted from that obtained from the less polar ICT excited state that forms in the absence of amine group rotation. Were the TICT state somewhat fluorescent (particularly in the "solid" materials studied here), dramatic spectral diffusion should be observable in the NR emission spectrum. Corresponding variations in the emission efficiency could then be the dominant cause of the observed signal fluctuations.[34] Humidity-dependent variations in the efficiency of TICT state formation would then lead to the observed humidity-dependent variations in the fluctuation rate.

To investigate the extent to which the TICT state and associated spectral diffusion might contribute to the signal fluctuations, numerous sequential single-molecule fluorescence spectra were recorded. The spectral shift as a function of time (250 ms resolution) was investigated for several NR molecules in PVA under controlled RH conditions. The time-dependent variations in the emission maximum for each molecule were obtained by fitting the data to Gaussian functions.[8] The standard deviations for each sequence of single-molecule emission maxima were then calculated and used to prepare the histograms shown in Figure 10. This process was made difficult in the studies at high RH by the increased rate of translational diffusion and photobleaching. However, the data clearly show the molecules exhibit relatively more spectral diffusion in PVA at higher RH.

Although this result is consistent with possible TICT state formation, the shift in the emission wavelength in time is much smaller than might be expected. For example, the planar and nonplanar configurations of perylene derivatives studied by

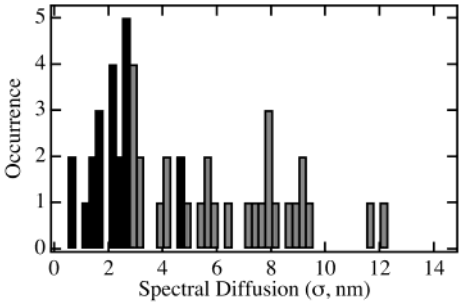

Figure 10. Spectral diffusion of single NR molecules in PVA under different RH conditions. Data are shown for NR in PVA at 31% RH (solid bars) and 65% RH (shaded bars). The extent of spectral diffusion for each molecule was classified by the standard deviation obtained for its emission maximum from a series of sequential spectra.

Stracke et al. yielded a separation of 80 nm between their emission maxima.[54] Because of its dramatic solvent sensitivity, the NR ICT and TICT states might be expected to yield a similar shift. Therefore, it is likely the increased spectral diffusion observed at higher RH results simply from increased variability in the properties of the local environments and all observed emission still arises from the ICT excited state. However, the observation of relatively long dark periods (i.e., several tens of milliseconds and longer) in the fluorescence transients and spectral diffusion studies are taken as evidence for time-dependent variations in the efficiency of TICT state formation. The associated molecular motions (i.e., amine group rotation) are relatively more free to occur in the more-polar, more-fluid, hydrated film environments at high RH.

IV. Conclusions

The effect of variations in the ambient RH on NR single-molecule signal fluctuations in PVA samples was studied. It was clearly shown that the extent and characteristic time scales of single-molecule signal fluctuations are dramatically dependent on ambient RH, when the molecules are entrapped in and/or on such hydrophilic materials. In contrast, only subtle RH-dependent effects were observed for relatively hydrophobic

samples such as PMMA. The possible causes for these signal fluctuations were investigated. In dry films at low RH, rapid (millisecond time scale) signal fluctuations were attributed to triplet blinking. In more hydrated films, triplet blinking was shown to play a reduced role. Signal fluctuations on both long and short time scales in films studied under higher RH conditions were shown to result partly from rotational and translational molecular motions. Although such motions were readily observable, it was also shown they were not the dominant contributors to the majority of the signal fluctuations. The dramatic moisture-dependent variations in signal fluctuations were attributed to the freeing of intramolecular motions on the NR molecules in hydrated environments. These motions, and the greater polarity of hydrated PVA environments, favor the formation of a nonfluorescent TICT excited state in NR. Variations in the efficiency of TICT state formation, and hence, the NR emission yield, are therefore concluded to be the primary cause of the majority of the observed signal fluctuations.

Acknowledgment. We gratefully acknowledge the financial support of the Army Research Office (DEPSCoR), Kansas State University, and 3M Co. in these studies.

References and Notes

(1) Moerner, W. E.; Kador, L. *Phys. Rev. Lett.* **1989**, *62*, 2535.
(2) Orrit, M.; Bernard, J. *Phys. Rev. Lett.* **1990**, *65*, 2716.
(3) Betzig, E.; Chichester, R. J. *Science* **1993**, *262*, 1422.
(4) Kelley, A. M. Single-Molecule Spectroscopy. In *Encyclopedia of Chemical Physics and Physical Chemistry*; Moore, J. H., Spencer, N. D., Eds.; Institute of Physics Publishing: Bristol, U.K., 2001; Vol. 3, p 2199.
(5) Brasselet, S.; Moerner, W. E. *Single Mol.* **2000**, *1*, 17.
(6) Weston, K. D.; Carson, P. J.; Metiu, H.; Buratto, S. K. *J. Chem. Phys.* **1998**, *109*, 7474.
(7) Deschenes, L. A.; Vanden Bout, D. A. *J. Phys. Chem. B* **2001**, *105*, 11978.
(8) Higgins, D. A.; Collinson, M. M.; Saroja, G.; Bardo, A. M. *Chem. Mater.* In Press.
(9) Bardo, A. M.; Collinson, M. M.; Higgins, D. A. *Chem. Mater.* **2001**, *13*, 2713. Bardo, A. M.; Collinson, M. M.; Higgins, D. A. *Chem. Mater.* **2001**, *13*, 3058.
(10) Hou, Y.; Bardo, A. M.; Martinez, C.; Higgins, D. A. *J. Phys. Chem. B* **2000**, *104*, 212.
(11) Marcus, R. A. *J. Phys. Chem.* **1990**, *94*, 4963.
(12) Brunschwig, B. S.; Ehrenson, S.; Sutin, N. *J. Phys. Chem.* **1987**, *91*, 4714.
(13) Deye, J. F.; Berger, T. A.; Anderson, A. G. *Anal. Chem.* **1990**, *62*, 615.
(14) Garbatski, U.; Folman, M. *J. Phys. Chem.* **1956**, *60*, 793.
(15) Hall, A. C. *J. Phys. Chem.* **1970**, *74*, 2742.
(16) Pashley, R. M.; Kitchener, J. A. *J. Colloid. Interface Sci.* **1979**, *71*, 491.
(17) Wang, J. Z.; Dillard, D. A.; Kamke, F. A. *J. Mater. Sci.* **1991**, *26*, 5113.
(18) Binggeli, M.; Mate, C. M. *Appl. Phys. Lett.* **1994**, *65*, 415.
(19) Guckenberger, R.; Heim, M.; Cevc, G.; Knapp, H. F.; Wiegrabe, W.; Hillebrand, A. *Science* **1994**, *266*, 1538.
(20) Leggett, G. J.; Davies, M. C.; Jackson, D. E.; Roberts, C. J.; Tendler, S. J. B.; Williams, P. M. *J. Phys. Chem.* **1993**, *97*, 8852.
(21) Fan, F.-R., F.; Bard, A. J. *Proc. Natl. Acad. Sci. U.S.A.* **1999**, *96*, 14222.
(22) Chen, W.-L.; Shull, K. R.; Papatheodrou, T.; Styrkas, D. A.; Keddie, J. L. *Macromolecules* **1999**, *32*, 136.
(23) Ebrahimzadeh, P. R.; Kubat, J. *J. Mater. Sci.* **1997**, *32*, 4227.
(24) Bhushan, B.; Dandavate, C. *J. Appl. Phys.* **2000**, *87*, 1201.
(25) Binggeli, M.; Mate, C. M. *J. Vac. Sci. Technol. B* **1995**, *13*, 1312.
(26) Israelachvili. *Acc. Chem. Res.* **1987**, *20*, 415.
(27) Frisbie, C. D.; Rozsnyai, L. F.; Noy, A.; Wrighton, M. S.; Lieber, C. M. *Science* **1994**, *265*, 2071.
(28) Hoh, J. H.; Cleveland, J. P.; Prater, C. B.; Revel, J.-P.; Hansma, P. K. *J. Am. Chem. Soc.* **1992**, *114*, 4917.
(29) Ha, T.; Enderle, T.; Chemla, D. S.; Selvin, P. R.; Weiss, S. *Chem. Phys. Lett.* **1997**, *271*, 1.
(30) Yip, W.-T.; Hu, D.; Yu, J.; Vanden Bout, D. A.; Barbara, P. F. *J. Phys. Chem. A* **1998**, *102*, 7564.
(31) English, D. S.; Furube, A.; Barbara, P. F. *Chem. Phys. Lett.* **2000**, *324*, 15.
(32) Weston, K. D.; Carson, P. J.; DeAro, J. A.; Buratto, S. K. *Chem. Phys. Lett.* **1999**, *308*, 58.
(33) Ambrose, W. P.; Moerner, W. E. *Nature* **1991**, *349*, 225.
(34) Lu, H. P.; Xie, X. S. *Nature* **1997**, *385*, 143.
(35) Sarkar, N.; Das, K.; Nath, D. N.; Bhattacharyya, K. *Langmuir* **1994**, *10*, 326.
(36) Golini, C. M.; Williams, B. W.; Foresman, J. B. *J. Fluoresc.* **1998**, *8*, 395.
(37) Dutta, A. K.; Kamada, K.; Ohta, K. *J. Photchem. Photobiol. A* **1996**, *93*, 57.
(38) Dickson, R. M.; Cubitt, A. B.; Tsien, R. Y.; Moerner, W. E. *Nature* **1997**, *388*, 355.
(39) Schmidt, T.; Schütz, G. J.; Baumgartner, W.; Gruber, H. J.; Schindler, H. *J. Phys. Chem.* **1995**, *99*, 17662.
(40) Schmidt, T.; Schütz, G. J.; Baumgartner, W.; Gruber, H. J.; Schindler, H. *Proc. Natl. Acad. Sci. U.S.A.* **1996**, *93*, 2926.
(41) Hou, Y.; Higgins, D. A. Unpublished.
(42) Mei, E.; Bardo, A. M.; Collinson, M. M.; Higgins, D. A. *J. Phys. Chem. B* **2000**, *104*, 9973.
(43) English, D. S.; Harbron, E. J.; Barbara, P. F. *J. Phys. Chem. A* **2000**, *104*, 9057.
(44) Gollnick, K.; Franken, T.; Fouda, M. F. R. *Tetrahedron Lett.* **1981**, *22*, 4049.
(45) Lakowicz, J. R. *Principles of Fluorescence Spectroscopy*, 2nd ed.; Plenum: New York, 1999.
(46) Wennmalm, S.; Rigler, R. *J. Phys. Chem. B* **1999**, *103*, 2516.
(47) Wirth, M. J.; Swinton, D. J. *Anal. Chem.* **1998**, *70*, 5264.
(48) Ha, T.; Glass, J.; Enderle, T.; Chemla, D. S.; Weiss, S. *Phys. Rev. Lett.* **1998**, *80*, 2093.
(49) Bartko, A. P.; Dickson, R. M. *J. Phys. Chem. B* **1999**, *103*, 3053.
(50) Fourkas, J. T. *Opt. Lett.* **2001**, *26*, 211.
(51) Hollars, C. W.; Dunn, R. C. *J. Chem. Phys.* **2000**, *112*, 7822.
(52) Jones, G.; Jackson, W. R.; Choi, C.; Bergmark, W. R. *J. Phys. Chem.* **1985**, *89*, 294.
(53) Krishna, M. M. G. *J. Phys. Chem. A* **1999**, *103*, 3589.
(54) Stracke, F.; Blum, C.; Becker, S.; Müller, K.; Meixner, A. J. *Chem. Phys. Lett.* **2000**, *325*, 196.